JOURNAL OF PROPULSION AND POWER
Vol. 15, No. 1, January–February 1999

Experimental Study of Sprays from Annular Liquid Jet Breakup

Xianguo Li*
University of Waterloo, Waterloo, Ontario N2L 3G1, Canada
and
Jihua Shen†
University of Victoria, Victoria, British Columbia V8W 3P6, Canada

An experimental investigation has been conducted to study the characteristics of sprays produced from the breakup of annular water jets exposed to inner airstreams, simulating twin-fluid atomization, by using phase Doppler anemometry. The spray characteristic parameters, such as droplet Sauter mean diameter (SMD), mean velocity, velocity fluctuation, and droplet number density, have been measured for various radial and axial locations and under various liquid and airflow velocities at the nozzle exit. The results indicate that the spray characteristic parameters are almost symmetric about the spray axis. At each axial spray cross section, the droplet mean axial velocity reaches the maximum value in the spray center and decreases from the spray center to the edge. Further, the droplet axial velocity has a jet-like self-similar spatial distribution along the radial and axial directions when normalized by appropriate reference parameters. Similar universal correlation is observed for the droplet fluctuation velocity and turbulent intensity as well. The SMD has a minimum value at the spray center and increases toward the spray periphery. The SMD at the spray centerline has a more complex variation in the downstream direction because of secondary atomization at high air velocity near the nozzle exit and droplet entrainment and migration farther downstream. The droplet number density has a radial distribution similar to that of the SMD, whereas its value at the spray center increases with the distance from the nozzle exit, and is reduced by the high air and liquid flow velocity.

Nomenclature

J = momentum of the air and liquid flow at a given spray cross section
r = radial location
U = droplet velocity in the spray envelope
U_a = air velocity at the nozzle exit
U_g = air velocity in the spray envelope
U_l = liquid velocity at the nozzle exit
u' = rms of turbulent fluctuation of the droplet velocity
x = radial direction of measurements
y = radial direction of measurements normal to x
z = axial distance from the nozzle exit
η = r/z
ϕ = volume fraction

Subscripts
a = air
l = liquid
max = maximum value

Introduction

TWIN-fluid atomization is used extensively in practical spray applications such as in spray drying operations[1] and power generation and propulsion systems.[2] The gas medium used for the promotion of liquid atomization is almost invariably the air for spray combustion applications such as in gas-turbine combustors that are found in small and large aircraft engines; hence, the name of airblast and air-assist atomization, depending on the relative velocity of the air and liquid fuel used. The disintegration of annular liquid jets in gas streams is one typical type of twin-fluid atomization widely employed in combustion engines. As Lefebvre[3] summarized, the principal factors governing the mean droplet sizes produced by twin-fluid atomization are the air and liquid velocity, air-to-liquid ratios, surface tension, and the geometrical design of the twin-fluid atomizers. The characteristics of the resulting sprays are known to have a significant impact on the efficiency of combustion processes and the level of pollutant formation and emission. Hence, a fundamental and practical knowledge of twin-fluid atomization and resultant spray characteristics is required for the performance improvement of related spray systems, and such knowledge is far from complete at the present time.

Theoretical studies have been conducted in the past on the instability and breakup process of an annular liquid jet, which is often referred to as annular liquid sheet. Crapper et al.[4] analyzed the instability of an inviscid annular liquid sheet moving in an inviscid and stationary gas medium, and examined the influence of the sheet thickness and radius on the unstable wave growth. Meyer and Weihs[5] investigated the capillary instability of a stationary viscous liquid sheet in a moving gas stream with a particular type of disturbance. The instability of a stationary viscous annular liquid sheet with different gas velocities for the inner and outer gas streams was considered by Lee and Chen.[6] However, only cases for inviscid liquids were analyzed. Shen and Li[7,8] studied the instability and breakup of a moving viscous annular liquid sheet, a situation that closely resembles the reality of practical applications, and investigated the effect of different inner- and outer-gas stream velocities, liquid sheet inner and outer radii, and various physical properties.

Received Dec. 23, 1997; presented as Paper 98-0729 at the AIAA 36th Aerospace Sciences Meeting, Reno, NV, Jan. 12–15, 1998; revision received June 22, 1998; accepted for publication June 25, 1998.
Copyright © 1998 by X. Li and J. Shen. Published by the American Institute of Aeronautics and Astronautics, Inc., with permission.

*Associate Professor, Department of Mechanical Engineering. E-mail: X6Li@mecheng1.uwaterloo.ca. Member AIAA.

†Graduate Student, Department of Mechanical Engineering; currently Assistant Professor, Department of Mechanical Engineering, University of Western Ontario, London, Ontario, Canada.

On the other hand, only limited experimental studies have been reported in literature on the detailed structures and characteristics of sprays resulting from the twin-fluid atomization. Lavergne et al.[9] investigated an annular liquid sheet, 400 μm thick, breaking up in two coflowing airstreams. The experiments were conducted using phase Doppler particle analyzer (PDPA) for spray characterization with limited data presented. Lai et al.[10] conducted an experimental study of droplet transport phenomena in sprays generated by a research simplex atomizer with and without atomizing air. A two-component PDPA was utilized to measure droplet sizes and velocities at different spatial locations in the spray with a fixed air-to-liquid mass ratio. The analysis of the histogram data showed that the transport of part of the smaller droplets from the outer region to the central region was the key process responsible for the increase in the droplet Sauter mean diameter (SMD), the droplet number density, and velocity fluctuations downstream.

In the present work, sprays from the disintegration of annular liquid sheets injected from an in-house-designed annular nozzle are investigated, and the effect of the airstream velocity is examined experimentally by using the phase Doppler anemometry. In what follows, the experimental apparatus, condition, and measurement procedure will be presented, followed by the results and discussion. This paper ends with conclusions drawn from the present study.

Experimental Apparatus, Condition, and Instrumentation

The nozzle used was designed in-house specifically for the present study. A smooth contraction contour for the liquid flow was adopted with the contraction ratio of about 1966 to provide a uniform velocity profile at the nozzle exit with minimal turbulent level. The smooth contraction was calculated based on the technique for the design of three-dimensional wind-tunnel contractions by Downie et al.[11] The nozzle configuration is shown in Fig. 1, and the details are given in Ref. 12. Because of the large contraction ratio for the liquid flow, the smooth nozzle contraction contour was formed by two elliptic arcs (AB and CD in Fig. 1), which was then connected by a straight line (BC). The annular region for the liquid flow was formed by inserting a circular pipe concentrically inside the contoured nozzle, and the thickness of the annular liquid sheet can be varied by using different sizes of the central pipes through which the air flows. The nozzle is shown schematically in Fig. 1, and the relevant nozzle dimensions are given in the figure caption, where L_B, L_C, and L_D denote the distance from points B, C, and D to the nozzle exit, respectively, and ϕ_A, ϕ_B, ϕ_C, and ϕ_D are the corresponding diameters. In addition, a set of fine-wire screens and honeycomb was placed at the inlet region of the nozzle for the liquid flow.

The entire test apparatus is schematically shown in Fig. 2. It consisted of an annular nozzle, as described earlier, with its

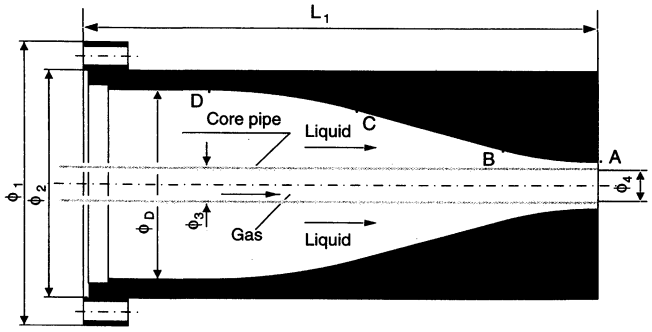

Fig. 1 Sectional view of the annular nozzle used in the present study. Main dimensions (unit: mm): L_1 = 105, ϕ_1 = 60, ϕ_2 = 48, core pipe o.d. ϕ_3 = 2.375, core pipe i.d. ϕ_4 = 1.588, annular o.d. at the nozzle exit ϕ_A = 2.540, ϕ_B = 10.8, L_B = 25, ϕ_C = 33, L_C = 58, ϕ_D = 40, and L_D = 80.

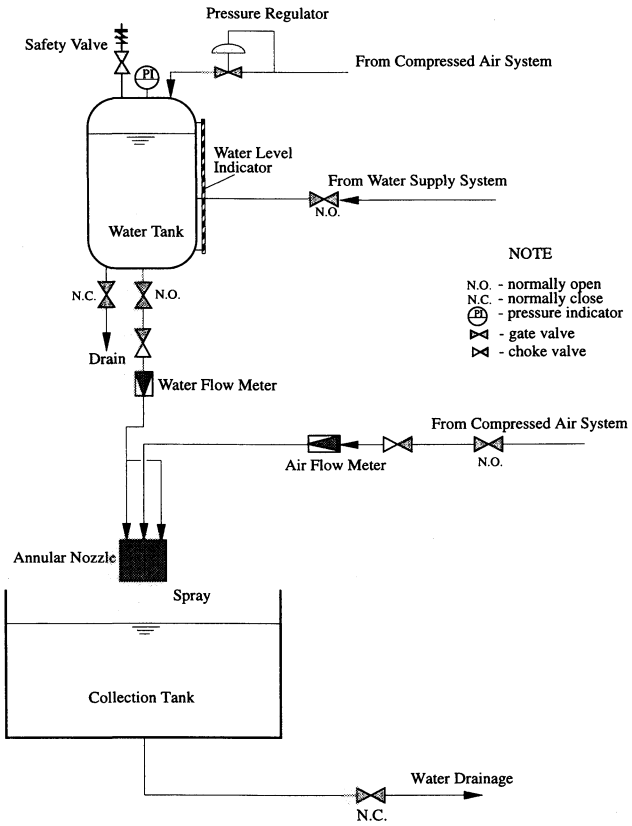

Fig. 2 Schematic of experimental setup.

annular section connected to the water-supply tank and the central core pipe linked to the compressed air supply. The water in the water tank was pressurized by the compressed house air supply to maintain steady water flow during experiments. Both water and airflow rates were measured by float flow meters. When the pressurized water is discharged from the annular section of the nozzle with its inner surface exposed to a coflowing airstream, an annular water sheet (or jet) is formed, which quickly breaks up into a cloud of droplets at a short distance downstream. The water droplets are collected by an open tank and then drained out through the floor drainage.

The annular section of the nozzle for the water flow has an o.d. of 2.540 mm and an i.d. of 2.375 mm at the nozzle exit, the i.d. of the core pipe is 1.588 mm for the airflow. Sprays from this annular nozzle are generated at four different water flow rates of 207, 388, 580, and 780 ml/min (corresponding to Reynolds numbers of 888, 1666, 2491, and 3351, respectively, based on the hydraulic diameter at the nozzle exit), and various airflow rates ranging from 22,900 to 35,722 ml/min (corresponding to Reynolds numbers of 2121–3309). The resulting sprays are characterized in terms of the droplet size and velocity distribution, spatial variations of the SMD, mean velocity and turbulent intensity, as well as the droplet number density.

A one-component particle dynamics analyzer (PDA), from Dantec Electronics, Inc., was used for the simultaneous measurement of droplet sizes and velocities. The operational principle for the PDA is similar to that of a conventional laser Doppler velocimeter (LDV), except that three photodetectors are used to resolve the ambiguity in the phase angle of the measured optical signals for the determination of droplet sizes.

The PDA system used in the present study was operated in a near-backscatter mode with the receiving optics unit mounted on the same side as the transmitting optics unit. The Dantec 55X transmitting optics used a helium–neon laser as the coherent light source. The laser beam was split, by a beam splitter, into two beams of equal intensity, and one beam was

shifted by a frequency of 40 MHz through a Bragg cell. The resulting two parallel beams were focused by the Dantec 55X57 transmitting lens of 310-mm focal length and the measurement volume was formed inside the spray droplet field. The scattered light from the individual droplets passing through the measurement volume was collected by the Dantec 57N10 PDA receiving optics, whose front lens of 310 mm focal length focused the collected light onto a slit aperture. This slit aperture acted as a spatial filter, allowing only the light scattered from the measurement volume to go through. Three 55X08 photomutipliers located behind the slit aperture in the receiving optic unit converted the light signal into an electric signal, which was transferred to the Dantec 58N10 PDA signal processor for data processing, and was then downloaded into a computer for data storage, analysis, and presentation.

The PDA transmitting and receiving optics were mounted on a three-dimensional traversing mechanism. The center of the sprays was determined experimentally as follows: before each set of measurements, the laser beams were focused, i.e., the measurement volume was positioned, at the nozzle centerline near the nozzle exit, then the PDA optics were lowered to the desired axial location of measurements. Both the axial and radial positions of each measurement were determined by the dial reading on the three-dimensional traversing mechanism. The dial reading had an accuracy of 0.0254 mm (0.001 in.).

Results and Discussion

Three groups of measurements were made during the experiments. First, measurements were made to examine the spray symmetry along one of the spray's radial direction x and its orthogonal direction y at the spray axial location of z = 151.6 mm for the fixed water flow rate of 388 ml/min and the airflow rate of 26,200 ml/min. The coordinate z has its origin located at the nozzle exit, pointing to the downstream direction of the liquid and airflow. The direction x is normal to, while the direction y is parallel to, the page in Fig. 2. Then the droplet size and axial velocity distributions were measured at up to 25 different locations along the radial direction x at the cross sections located at z = 37.3, 75.4, 113.5, 151.6, and 177.0 mm, respectively. For all of the radial profiles presented, the left side of the figure represents the laser entrance where the laser beam blockage by the spray was low. Finally, the effects of water and air velocities were investigated by taking measurements up to 20 locations along the spray axis z for different water and airflow rates. The details of the measurements along with the original data are given elsewhere.[12] An example of the droplet velocity and size histogram is shown in Fig. 3.

Spray Symmetry Assessment

Figure 4 shows the arithmetic mean axial velocity of droplets measured along the two orthogonal radial directions at the axial location of z = 151.6 mm downstream of the nozzle exit. It is seen that the mean velocity reaches the maximum value at the spray centerline, and decreases toward the spray edges as the spray spreads out. The air entrainment from the surrounding to the spray region is responsible for this behavior of the mean velocity distribution. The velocity profile is nearly

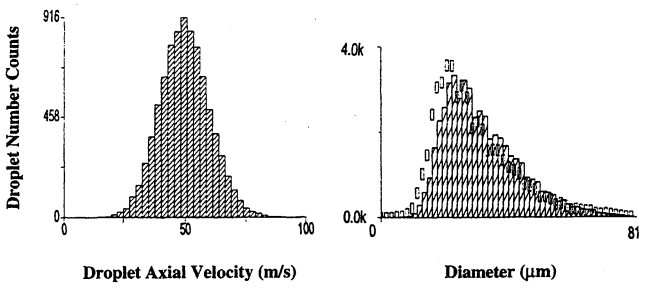

Fig. 3 Example of the droplet velocity and size histogram.

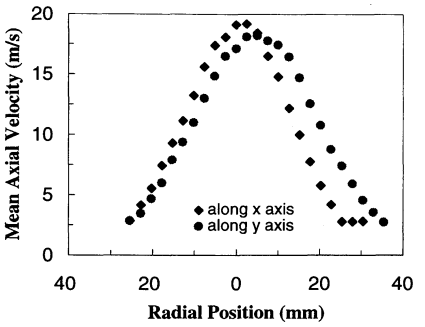

Fig. 4 Distribution of droplet mean axial velocity along two orthogonal radial directions x and y. Water velocity: U_l = 10.15 m/s, air velocity: U_a = 220.6 m/s, and axial location from the nozzle exit: z = 151.6 mm.

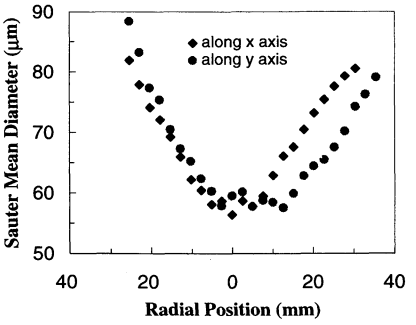

Fig. 5 Distribution of droplet SMD along two orthogonal radial directions x and y. Water velocity: U_l = 10.15 m/s, air velocity: U_a = 220.6 m/s, and axial location from the nozzle exit: z = 151.6 mm.

symmetric about the spray centerline z. The small off-the-center distribution may be attributed to the fact that the nozzle positions might not be exactly the same before and after it was rotated 90 deg during the measurements along the two orthogonal radial directions, x and y, although much attention was paid to it. It may be pointed out that the mean droplet axial velocities along both directions exhibit a typical Gaussian-type variation, similar to those observed for sprays formed from plane liquid sheet breakup[13] and from the annular liquid sheet breakup.[9]

The variation of the SMDs, shown in Fig. 5, is nearly symmetric about the spray axis. It is slightly off the centerline similar to the velocity profiles presented earlier. It is clear that the SMD increases from the spray central region to the periphery. The larger droplets have higher momentum, tend to follow their own trajectories, and are less affected by the air entrainment motion near the spray edges. Small droplets are easily entrained to the central region; hence, showing a nearly uniform SMD distribution there because of the inner airflow from the core pipe. This spatial variation differs from the observations for sprays from the breakup of cylindrical liquid jets surrounded by an airstream[10] and of the sandwich type of plane liquid sheets,[13] where small droplets are typically present in the center of the spray.

Spatial Distributions of Droplet Properties

The spatial variations of the spray characteristics are presented in Figs. 6–11 for the droplet mean axial velocity, rms of the velocity fluctuations, turbulent intensity, SMD, and droplet number density. These results were measured at various radial positions at five different axial locations under a fixed flow condition. It is seen from the figures that all of the spray characteristics are essentially symmetric about the spray axis.

Figure 6 gives the spatial distribution of the droplet mean axial velocity U. It is clear that the droplet velocity reaches a maximum value at the spray centerline and then decreases monotonically from the center to the spray boundary. The var-

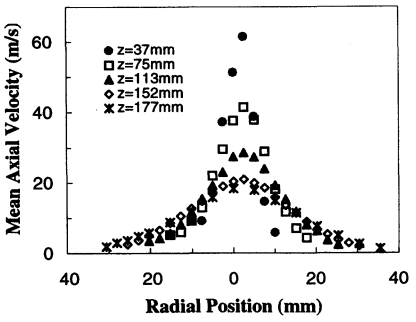

Fig. 6 Spatial distribution of the droplet mean axial velocity for the water velocity of U_l = 10.15 m/s and air velocity of U_a = 220.6 m/s.

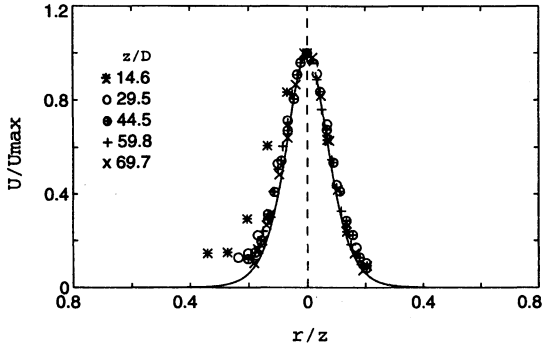

Fig. 7 Self-similarity of the droplet mean axial velocity. Water velocity: U_l = 10.15 m/s, and air velocity: U_a = 220.6 m/s. ——, Eq. (1).

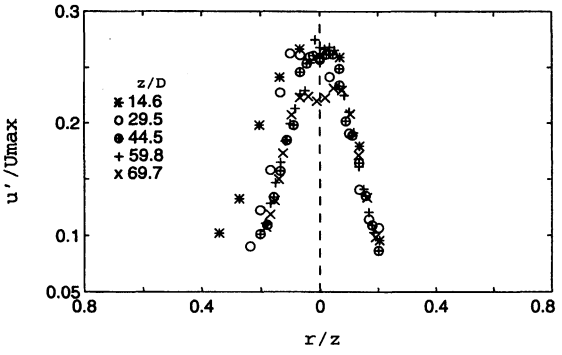

Fig. 8 Self-similarity of the turbulent fluctuation of the droplet axial velocity. Water velocity: U_l = 10.15 m/s, and air velocity: U_a = 220.6 m/s.

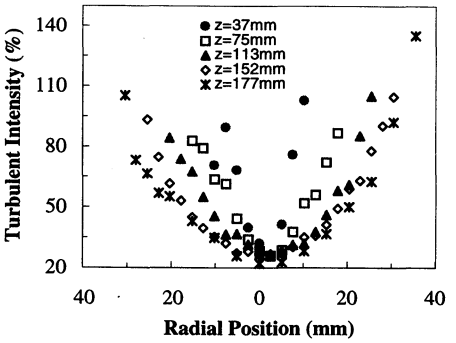

Fig. 9 Spatial distribution of the turbulent intensity. Water velocity: U_l = 10.15 m/s, and air velocity: U_a = 220.6 m/s.

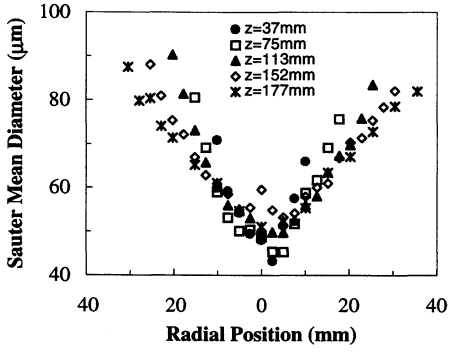

Fig. 10 Spatial distribution of the droplet SMD. Water velocity: U_l = 10.15 m/s, and air velocity: U_a = 220.6 m/s.

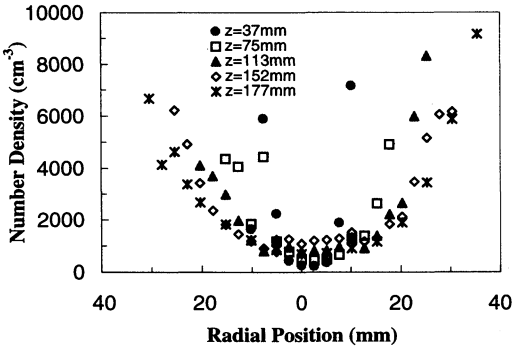

Fig. 11 Spatial distribution of the droplet number density. Water velocity: U_l = 10.15 m/s, and air velocity: U_a = 220.6 m/s.

iation of the velocity profile along the spray axis z in the downstream direction indicates the expansion of the spray region caused by the effect of spray–air interaction and air entrainment. Along the downstream direction, the variation of the droplet velocity near the central region is just opposite to that near the edge. Near the center, the axial mean velocity decreases as the distance from the nozzle increases, whereas close to the edge it increases downstream. In other words, the droplets closer to the nozzle exit have higher velocities than those farther downstream in the central region. Whereas, near the spray boundary, the droplets closer to the nozzle exit have lower velocities than those farther downstream. This is similar to the characteristics of sprays from plane liquid sheet breakup.[13] At the nozzle exit, the initial larger velocity difference, i.e., 211 m/s, between the liquid and the core airflow results in high velocities of the droplets because of strong momentum transfer and the small sizes of the droplets. After a certain distance downstream of the nozzle exit, the droplets are accelerated to the velocity of the core air, which slows down as a result of the loss of its momentum to the droplets and the entrained surrounding air. Then, as the droplets and the coflowing air are transported farther downstream and spread out, they are decelerated because of the continual air entrainment from the surroundings. Thus, the velocity profile flattens as the spray region expands downstream along the spray axis.

The foregoing discussion suggests that sufficiently downstream of the nozzle exit, the spray droplets would move at a velocity nearly the same as that of the continual phase air. Hence, the velocity distribution should behave like a single-phase jet, exhibiting a self-similar universal velocity profile. That is, the droplet mean velocity at each axial location, normalized by its maximum value at the centerline, should be a function of the radial location normalized by the axial distance from the nozzle exit,[14] or

$$\frac{U(r, z)}{U_{\max}(z)} = f\left(\frac{r}{z}\right) \approx \operatorname{sech}^2\left(10.4\,\frac{r}{z}\right) \qquad (1)$$

where $U(r, z)$ is the axial mean velocity, and $U_{\max}(z)$ is the maximum velocity occurring at $r = 0$. Equation (1) is originally

obtained for a single-phase round and turbulent jet.[14] As shown in Fig. 7, the measured data of the droplet axial mean velocity fall reasonably well onto the self-similar universal velocity profile given by Eq. (1). Figure 7 also indicates that the velocity profile does not become self-similar until the distance from the nozzle exit z is about 29.5 times the nozzle diameter D ($=\phi_A$, the o.d. of the nozzle at the nozzle exit). However, for a single-phase turbulent round jet, self-similarity in the velocity profile begins at z/D around 20. Clearly, the presence of the dispersed droplets, which have smaller initial velocities or momentum, has delayed the development of the self-similar velocity distribution.

As for the single-phase turbulent jet, the turbulent component (rms or u') of the droplet axial velocity takes longer to develop than the mean velocity profile. As shown in Fig. 8, it is not similar at $z/D = 29.5$, and does not become similar until $z/D = 44.5$. Note that nonsimilar variation of the turbulent component occurs in the spray central region.

Figure 9 indicates that the turbulent intensity, u'/U, has the lowest value in the center and increases toward the spray edge at every axial cross section. It is because the axial mean velocity U, as given in Fig. 6, is the largest at the center and decreases to zero at the edges, and this variation dominates over the corresponding change of the velocity fluctuations u' shown in Fig. 8. It is also seen that at fixed radial locations the turbulent intensity decreases as the distance from the nozzle exit is increased. Also notice the high levels of turbulence near the spray edges. Because

$$\frac{u'}{U} = \frac{u'/U_{\max}}{U/U_{\max}} = \text{fcn}\left(\frac{r}{z}\right) \tag{2}$$

considering the self-similar distributions of $U/U_{\max}$ and $u'/U_{\max}$ given in Figs. 7 and 8, respectively, the turbulent intensity will also develop a self-similar universal profile.

The SMD of the droplets is presented in Fig. 10 as a function of the radial position for the measurements taken at five different axial locations. Referring back to the variation of the axial mean velocity shown in Fig. 6, it becomes evident that the variations of the droplet sizes and velocities are consistent with each other in the sense that smaller droplets, having smaller inertia, have been entrained by the high-velocity core airstream and are accelerated to higher velocities in the central region of the spray, and larger droplets, having larger inertia, have smaller velocities in the outer region of the spray. On the other hand, one might explain that the high mean and fluctuation component of the droplet velocities in the spray central region results in small droplets there because high shear and aerodynamic interaction between the liquid and gas phase are known to be beneficial for the production of small droplets, as predicted by the linear instability theory and other experimental observations.

The variation of the droplet number density as a function of the radial position is shown in Fig. 11. It is seen that the number density has a minimum value at the spray center, and increases monotonically toward the spray edge, very similar to the variation of the droplet size shown earlier. Hence, at each axial spray plane, there are always fewer small droplets in the central region than the number of the relatively large droplets near the spray boundary. This is because there is an air core inside of the annular liquid sheet. The presence of the air core results in a dilute spray in the central region. It is also seen that some increase in the average droplet size (the SMD) with the axial distance occurs near the central region, similar to that observed by Lavergne et al.[9] As will be shown later, this is mainly because of relatively large droplets migrating toward the central region.

Effects of Water and Air Velocities

To further investigate the characteristics of the sprays formed from the breakup of annular liquid sheets in a coflowing airstream, the droplet mean axial velocity, SMD, and droplet number density were measured at different axial locations with various water and air velocities at the nozzle exit. The representative results are presented in Figs. 12–19, and the variation of the spray characteristics along the spray axis downstream is shown for pairs of water and air velocities at the nozzle exit (U_l, U_a).

Figure 12 shows the droplet mean axial velocity at the spray centerline, $U_{\max}$, for various liquid and airflow rates. It is clear that $U_{\max}$ decreases downstream, although the droplet velocity value depends on the magnitude of water and air velocities at the nozzle exit. This decrease in the axial velocity results mainly from the boundary-layer growth and the entrainment of the ambient air. Rapid mixing of the spray droplets with the surrounding airstream and the resulting momentum exchange lead to the deceleration of droplets in the spray central region. At a fixed axial position, the droplet mean velocity increases with the air velocity for a fixed water velocity. For example, at the water velocity of $U_l = 5.41$ m/s, the mean velocity curve in Fig. 12 moves up as the air velocity is increased from 192.8 to 276.7 m/s. Clearly, when the air velocity is higher, the momentum transferred from the core airstream to the dispersed phase or droplets is larger. Therefore, the droplet velocity is higher. However, the effect of the air velocity on the droplet velocity becomes smaller when the water velocity is increased. This is because the momentum is proportional to the density, and the liquid water density is nearly a thousand times larger than the air. It is also noticed that similar variation occurs for the droplet axial mean velocity with the water velocity at a fixed air velocity. For a fixed air velocity, e.g., $U_a = 220.6$ m/s, an increase in the water velocity causes the droplet velocity to increase, but the increase is more significant for low values of the water velocity (from $U_l = 5.41$ to 10.15 m/s) than for the larger U_l (from $U_l = 10.15$ to 15.17 m/s). The effect of

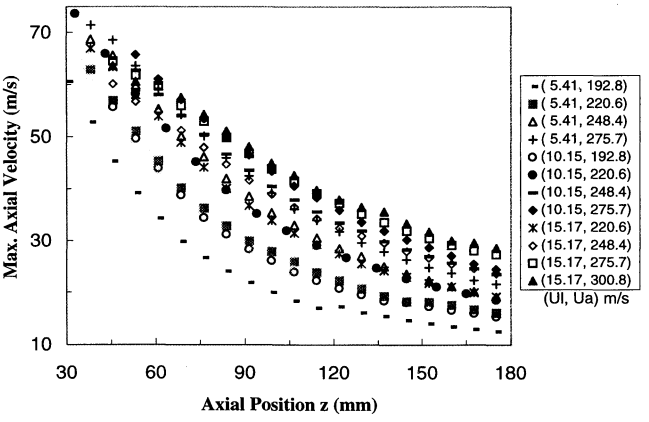

Fig. 12 Effects of the water and air velocities at the nozzle exit on the droplet mean axial velocity along the spray axis.

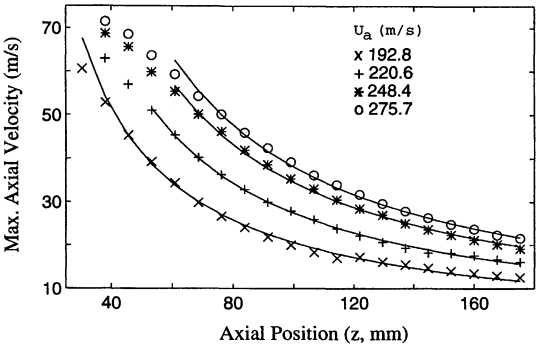

Fig. 13 Correlation for the self-similarity of the maximum droplet mean axial velocity. Water velocity: $U_l = 5.41$ m/s. ——, correlation, Eq. (5).

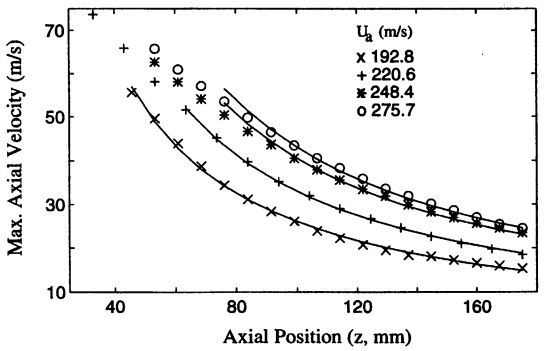

Fig. 14 Correlation for the self-similarity of the maximum droplet mean axial velocity. Water velocity: U_l = 10.15 m/s. ——, correlation, Eq. (5).

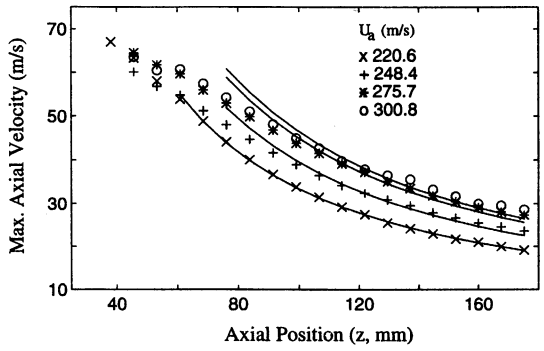

Fig. 15 Correlation for the self-similarity of the maximum droplet mean axial velocity. Water velocity: U_l = 15.17 m/s. ——, correlation, Eq. (5).

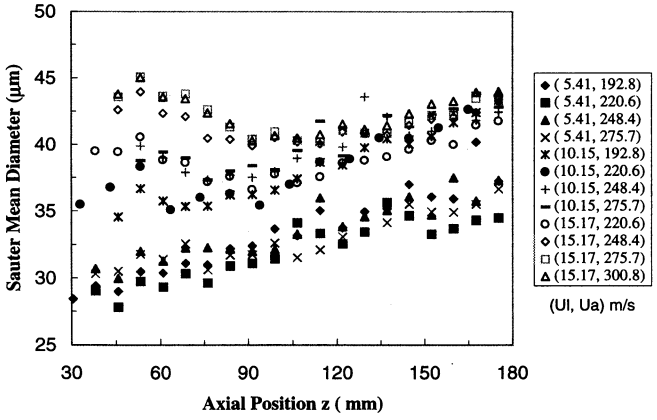

Fig. 16 Effects of water and air velocities at the nozzle exit on the droplet SMD along the spray axis.

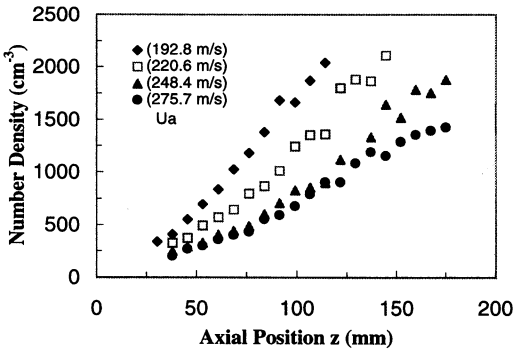

Fig. 17 Effects of water and air velocities at the nozzle exit on the droplet number density along the spray axis. Water velocity: U_l = 5.41 m/s.

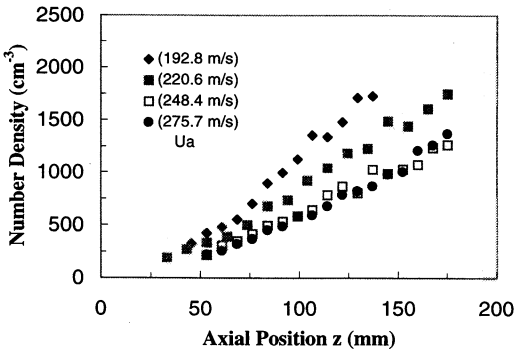

Fig. 18 Effects of water and air velocities at the nozzle exit on the droplet number density along the spray axis. Water velocity: U_l = 10.15 m/s.

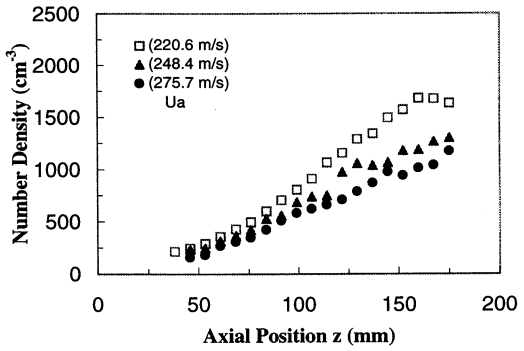

Fig. 19 Effects of water and air velocities at the nozzle exit on the droplet number density along the spray axis. Water velocity: U_l = 15.17 m/s.

the water velocity becomes smaller when the air velocity is increased.

An analysis can be carried out for the variation of the maximum axial velocity U_{max} similar to the radial distribution of the axial mean velocity presented earlier. According to the conservation of momentum, the momentum of the spray droplets and the coflowing airstream J must remain constant at each cross section of the spray. That is

$$J = \int \phi_a \rho_a U_g^2 \, dA + \int \phi_l \rho_l U^2 \, dA = \text{const} = J_0 \qquad (3)$$

where J_0 represents the sum of the momentum of the annular liquid flow and core airstream at the nozzle exit; ρ_a and ρ_l are the density of the air and liquid, respectively; ϕ_a and ϕ_l are the volume fraction of the air and liquid, respectively, at the specific location of (r, z), and $\phi_a + \phi_l = 1$. With the results presented in Figs. 6–9, it is reasonable to assume that sufficiently downstream of the nozzle exit, the liquid droplet and the air velocity are nearly the same ($U = U_g$), and lie in the self-similar region as discussed in the previous section. Then, from the self-similar universal velocity profile given in Eq. (1), Eq. (3) can be rearranged as follows, noting that the area element $dA = 2\pi r \, dr$ for the axisymmetric spray droplets and air motion:

$$\frac{U_{max}}{\left(\frac{J}{\rho_a}\right)^{1/2}} = \frac{1/z}{\left\{\int_0^\infty \left[1 + \phi_l\left(\frac{\rho_l}{\rho_a} - 1\right)\right] f^2(\eta) 2\pi\eta \, d\eta\right\}^{1/2}} \qquad (4)$$

where $\eta = r/z$. By definition, the volume fraction of the liquid is $0 \le \phi_l \le 1$. In reality, ϕ_l is typically very small in the dilute spray region, where the self-similar velocity profile is valid. However, the density ratio of the liquid to the air is large, such

that the term $\phi_l(\rho_l/\rho_a - 1)$ may not be negligible unless it is sufficiently far downstream of the nozzle exit. However, if the effect is small, or if ϕ_l also has a self-similar spatial distribution like the velocity profile, i.e., $\phi_l = \phi_l(\eta)$, then the denominator in Eq. (4) reduces to a constant. Therefore, Eq. (4) becomes

$$U_{\max} = C(J/\rho_a)^{1/2}/z \tag{5}$$

For a single-phase round turbulent jet, i.e., $\phi_l = 0$, $C = 7.4$.[14] For the present two-phase flow, C is expected to depend on the conditions of the annular liquid flow and the core airstream at the nozzle exit, as suggested by Eq. (4). Physically, the momentum of the high-velocity core airstream available at the nozzle exit is not only transferred to entrain the surrounding quiescent air, but is also used to help the liquid atomization and accelerate the resultant droplets to a higher velocity than the liquid velocity at the nozzle exit before deceleration starts.

The experimentally measured data shown in Fig. 12 have been used to determine the constant C for the present two-phase flow, and the obtained values of C for various water and airflow conditions at the nozzle exit are presented in Table 1 along with the standard deviation. It is seen that the correlation coefficient C varies slightly with the water and air velocity at the nozzle exit, and its numerical value is very close to the value of 7.4 obtained for a single-phase round jet. This indicates that the assumption made earlier concerning the liquid volume fraction is realistic for the present flow situations. Figures 13–15 show a comparison between the correlation [Eq. (5)], with the experimentally measured maximum velocity at the spray centerline for various nozzle exit flow conditions. It is clear that Eq. (5) correlates the data very well, except for the data points close to the nozzle exit. This is because Eq. (5) is derived based on the self-similar velocity profile of Eq. (1), which is only valid at a distance sufficiently far downstream of the nozzle exit. As expected, this critical distance is influenced by the nozzle exit flow conditions of the liquid and the air, which is clearly shown in Figs. 13–15.

Figure 16 presents the SMD of the droplets at the spray centerline as a function of the downstream distance from the nozzle exit. These results were measured at different axial locations for three fixed water velocities (U_l = 5.41, 10.15, and 15.17 m/s) and five different air velocities (U_a = 192.8, 220.6, 248.0, 275.7, and 300.8 m/s). The data points shown in the figure can be classified into three groups. One group of the lowest SMD values is the result for the water velocity of 5.41 m/s. The group of data points in the upper part of the figure is for the water velocity equal to 15.17 m/s. The group of data points in between is for the water velocity of 10.15 m/s. It is seen that the effects of the water and air velocity on the SMD are not as obvious and well-defined as on the droplet mean axial velocity. However, the SMD has, in general, a global increase with the increase in the water velocity, and for a fixed water velocity, the air velocity shows a small effect on the SMD. The SMD for U_l = 5.41 m/s increases downstream because of air entrainment and the droplet migration toward the spray central region as evidenced in Fig. 17. The SMD for U_l of 10.15 m/s seems to remain more or less constant until the downstream distance of approximately 90 mm, after that it starts to increase gradually. For the liquid velocity of 15.17 m/s, the SMD decreases initially until $z \approx 100$ mm, and then continues the general trend of the increase with the downstream distance. This initial decrease in the SMD with z can be attributed to the secondary atomization or the droplet breakup in the high-velocity core airstream, because the Weber number based on the relative velocity measured is estimated to exceed the critical value of 10. Figure 16 also indicates that air velocity seems to slightly increase the SMD at a fixed axial location for all measurements obtained at the three water velocities considered in this study. This is because the high-velocity core airstream reduces the droplet population in the central spray region resulting from a dilution effect, and at the same time it enhances the entrainment of the surrounding air and droplets as well. As a result, the SMD along the spray centerline is increased by the relatively large droplets entrained there.

Table 1 Correlation coefficient C in Eq. (5)[a]

U_l, m/s	U_a, m/s	Coefficient C	Standard deviation, %
5.41	192.83	6.943	7.25
	220.61	8.240	1.98
	248.40	9.340	2.60
	275.72	9.380	2.75
10.15	192.83	7.385	3.28
	220.61	8.594	1.32
	248.40	9.740	2.67
	275.72	9.590	2.66
15.17	220.61	7.293	1.03
	248.40	8.140	4.57
	275.72	8.735	5.74
	300.79	8.583	6.86

[a]Plus associated uncertainties for various water and airflow velocities at the nozzle exit.

The number density of the droplets along the spray centerline is presented in Figs. 17–19 for the three different water velocities involved. It is seen that the number densities increase with the downstream distance from the nozzle exit, mainly because of the droplet entrainment and migration. At a fixed axial location it decreases with the central core air velocity for a fixed water flow caused by the dilution of the spray. It is also observed that the number density at a fixed axial location and a fixed airflow decreases as the water velocity at the nozzle exit is increased. This is primarily because the droplet sizes, as shown in Fig. 16, increase with the water flow, and at the same time, the larger droplets, having larger inertia, tend to keep their original trajectories and are less inclined to be entrained to the central region of the spray.

Conclusions

The characteristics of sprays produced from the breakup of annular water jets exposed to inner airstreams have been investigated experimentally by using phase Doppler anemometry. The spray characteristic parameters, such as droplet SMD, mean velocity, velocity fluctuation, and droplet number density, have been measured for various radial and axial locations and under various liquid and airflow velocities at the nozzle exit. The results indicate that the spray characteristic parameters are almost symmetric about the spray axis. At each axial spray cross section, the droplet mean axial velocity reaches the maximum value in the spray center and decreases from the spray center to the edge. Further, the droplet axial velocity has a jet-like self-similar spatial distribution along the radial and axial directions when normalized by appropriate reference parameters. Similar universal correlation is observed for the droplet fluctuation velocity and turbulent intensity as well. The SMD has a minimum value at the spray center and increases toward the spray periphery. The SMD at the spray centerline has a more complex variation in the downstream direction because of secondary atomization at high air velocity near the nozzle exit and droplet entrainment and migration farther downstream. The droplet number density has a radial distribution similar to that of the SMD, whereas its value at the spray center increases with the distance from the nozzle exit, and is reduced by the high air and liquid flow velocity.

Acknowledgment

The financial support of the Natural Sciences and Engineering Research Council of Canada is gratefully acknowledged.

References

[1]Masters, K., *Spray Drying Handbook*, 4th ed., Wiley, New York, 1985.

[2]Lefebvre, A. H., *Atomization and Sprays*, Hemisphere, New York, 1989.

[3]Lefebvre, A. H., "Twin-Fluid Atomization: Factors Influencing Mean Drop Size," International Conference on Liquid Atomization and Spray Systems, Paper D, Gaithersburg, MD, July 1991.

[4]Crapper, G. D., Dombrowski, N., and Pyott, G. A. D., "Kelvin-Helmholtz Wave Growth on Cylindrical Sheets," *Journal of Fluid Mechanics*, Vol. 68, No. 3, 1975, pp. 497–502.

[5]Meyer, J., and Weihs, D., "Capillary Instability of an Annular Liquid Jet," *Journal of Fluid Mechanics*, Vol. 179, No. 6, 1987, pp. 531–545.

[6]Lee, J. G., and Chen, L. D., "Linear Stability Analysis of Gas-Liquid Interface," *AIAA Journal*, Vol. 29, No. 10, 1991, pp. 1589–1595.

[7]Shen, J., and Li, X., "Instability of an Annular Viscous Liquid Jet," *Acta Mechanica*, Vol. 114, No. 1–4, 1996, pp. 167–183.

[8]Shen, J., and Li, X., "Breakup of Annular Viscous Liquid Jets in Two Gas Streams," *Journal of Propulsion and Power*, Vol. 12, No. 4, 1996, pp. 752–759.

[9]Lavergne, G., Trichet, P., Hebrard, P., and Biscos, Y., "Liquid Sheet Disintegration and Atomization Process on a Simplified Airblast Atomizer," *Journal of Engineering for Gas Turbine and Power*, Vol. 115, No. 3, 1993, pp. 461–466.

[10]Lai, W. H., Yang, H., Hong, C. H., and Wang, M. R., "Droplet Transport in Simplex and Air-Assisted Sprays," *Atomization and Sprays*, Vol. 6, No. 1, 1996, pp. 27–49.

[11]Downie, J. H., Jordinson, R., and Barnes, F. H., "On the Design of Three-Dimensional Wind Tunnel Contractions," *Aeronautical Journal*, Vol. 88, No. 3, 1984, pp. 287–295.

[12]Shen, J., "Formation and Characteristics of Sprays from Annular Liquid Jet Breakup," Ph.D. Dissertation, Univ. of Victoria, Victoria, BC, Canada, May 1997.

[13]Mansour, A., and Chigier, N., "Disintegration of Liquid Sheets," *Physics of Fluids A*, Vol. 2, No. 5, 1990, pp. 706–719.

[14]White, F. M., *Viscous Fluid Flow*, 2nd ed., McGraw–Hill, New York, 1991.

SDM: The Gateway to Aerospace

40th AIAA/ASME/ASCE/AHS/ASC Structures, Structural Dynamics, and Materials Conference and Exhibit

AIAA/ASME/AHS Adaptive Structures Forum

AIAA Forum on Non-Deterministic Approaches

12-15 April 1999
St. Louis, Missouri
Hyatt Regency St. Louis at Union Station

Early Registration Deadline:

12 March 1999

AIAA
American Institute of Aeronautics and Astronautics

For a free preliminary program or to register, contact AIAA Customer Service at:
Phone: 800/639-2422 or 703/264-7500 (outside U.S.)
Fax: 703/264-7657
E-mail: custserv@aiaa.org
Or visit our Web site for the most up-to-date information at www.aiaa.org

Receive free conference registration when you attend one of these courses:*

- Introduction to Aircraft Design Loads
- Satellite Structural Systems—Design and Analysis
- Aeroelasticity: State-of-the-Art Practices

Includes admittance to conference technical sessions and exhibits only.